Progress in development of SiC-based joints resistant to neutron irradiation

Elsevier Editorial System(tm) for Journal of the European Ceramic Society
Manuscript Draft

Manuscript Number:

Title: Progress in development of SiC-based joints resistant to neutron irradiation

Article Type: Full Length Article

Keywords: Silicon carbide; joining; neutron irradiation

Corresponding Author: Dr. Takaaki Koyanagi, Ph.D.

Corresponding Author's Institution: Oak Ridge National Laboratory

First Author: Takaaki Koyanagi, Ph.D.

Order of Authors: Takaaki Koyanagi, Ph.D.; Yutai Katoh; Tatsuya Hinoki; Charles Henager; Monica Ferraris; Salvatore Grasso

Abstract: This study fills a knowledge gap regarding neutron-irradiation resistance of SiC joints for nuclear applications, by investigating high-dose neutron irradiation effects on the strength of selected joints and low-dose neutron irradiation effects on recently developed joints fabricated by state of the art processing methods. The joining methods used for the high-dose radiation study included pressure-assisted liquid-phase sintering (LPS) of SiC nanopowder, pressureless calcia-alumina glass ceramics joining, and reaction sintering of Ti-Si-C powders with hot-pressing. The joints were neutron-irradiated at 530°C to 20 displacements per atom (dpa). Other joining methods included low-pressure LPS of cold-pressed SiC green body, pressureless reaction sintered Ti-Si-C powder joint, spark plasma-sintered Ti diffusion bond, and hot-pressed Ti diffusion bond, which were irradiated at ~500°C to ~2 dpa. There was no notable degradation of torsional strengths of the joints following the high-dose irradiation. The irradiation-induced degradation at low neutron dose was highly dependent on joint type.

Suggested Reviewers: Qing Huang
Ningbo Institute of Materials Technology & Engineering, Chinese Academy of Sciences
huangqing@nimte.ac.cn
His expertise includes nuclear materials, joining and irradiation effects.

Cédric SAUDER
CEA
cedric.sauder@cea.fr
One of the leading experts on development of SiC materials for nuclear applications in Europe

Weon-Ju Kim
Korea Atomic Energy Research Institute
weonjkim@kaeri.re.kr
A leading scientist developing SiC materials for nuclear structural applications in Korea

OAK RIDGE NATIONAL LABORATORY
MANAGED BY UT-BATTELLE FOR THE DEPARTMENT OF ENERGY

September 11, 2019

Professor R.I. Todd
Senior Editor, Journal of the European Ceramic Society
Dept. of Materials, University of Oxford, 16 Parks Road, OX1 3PH, Oxford, UK

Dear Professor R.I. Todd,

I would like to submit for publication in the *Journal of the European Ceramic Society* the attached paper entitled "*Progress in development of SiC-based joints resistant to neutron irradiation*".

Our aim was to fill a knowledge gap regarding neutron irradiation resistance of SiC joints by investigating high-dose neutron irradiation effects on the strength of selected joints and low-dose neutron irradiation effects on recently developed joints fabricated by state of the art processing methods. Joining is a key technology for the development of SiC based core structures for nuclear applications.

We demonstrated that the selected SiC joints retained strength after neutron irradiation for 350 days. In addition, the joining process was improved by reducing applied stress or processing time for specific joint types. Such improved joints also retained strength following low-dose neutron irradiation. We explained the response of the joints to irradiation in details based on microstructural observations.

We believe that our findings will be of great interest to readers of your journal because development of SiC materials is currently a very active topic for nuclear structural applications.

I look forward to hearing from you.

Yours sincerely,

Takaaki Koyanagi, PhD
Research Associate
Materials Science and Technology Division
Oak Ridge National Laboratory
1 Bethel Valley Road, A-164 Building 4500S
Oak Ridge, TN 37831-6140 USA

Email: koyanagit@ornl.gov
TEL: +1-865-574-8764

***Summary of Novel Conclusions**

Significant progress in development of SiC joint for nuclear applications has been made; selected SiC joints retained strength after neutron irradiation for 350 days. The joining processes were also improved.

Progress in development of SiC-based joints resistant to neutron irradiation*

Takaaki Koyanagi[1†], Yutai Katoh[1], Tatsuya Hinoki[2], Charles Henager[3], Monica Ferraris[4], Salvatore Grasso[5]

[1] Oak Ridge National Laboratory, Oak Ridge, TN, 37831, USA
[2] Institute of Advanced Energy, Kyoto University, Uji, Kyoto, 611-0011, Japan
[3] Pacific Northwest National Laboratory, Richland, WA, 99352, USA
[4] Department of Applied Science and Technology, Politecnico di Torino, Torino, 10129, Italy
[5] Southwest Jiaotong University, 610031 Chengdu, PR China

Abstract

This study fills a knowledge gap regarding neutron-irradiation resistance of SiC joints for nuclear applications, by investigating high-dose neutron irradiation effects on the strength of selected joints and low-dose neutron irradiation effects on recently developed joints fabricated by state of the art processing methods. The joining methods used for the high-dose radiation study included pressure-assisted liquid-phase sintering (LPS) of SiC nanopowder, pressureless calcia-alumina glass ceramics joining, and reaction sintering of Ti-Si-C powders with hot-pressing. The joints were neutron-irradiated at 530°C to 20 displacements per atom (dpa). Other joining methods included low-pressure LPS of cold-pressed SiC green body, pressureless reaction sintered Ti-Si-C powder joint, spark plasma–sintered Ti diffusion bond, and hot-pressed Ti diffusion bond, which were irradiated at ~500°C to ~2 dpa. There was no notable degradation of torsional strengths of the joints following the high-dose irradiation. The irradiation-induced degradation at low neutron dose was highly dependent on joint type.

Keywords: Silicon carbide, joining, neutron irradiation

† Corresponding author address: Oak Ridge National Laboratory, 1 Bethel Valley Road, Oak Ridge, TN 37831-6140, USA.
Email: koyanagit@ornl.gov, Phone: +1-865-574-8764, Fax: +1-865-241-3650

1. Introduction

Joining is an essential technology for fabricating large and/or complex-shape components. For the development of silicon carbide (SiC) based materials for nuclear applications, it is also recognized as a key technology [1,2]. A fusion blanket, for example, requires the assembly of SiC based components of various shapes [3,4]. Joining complex-shape components becomes feasible when low joining pressure is used. In the case of SiC composite fuel cladding for light water reactors, the development of end-plug sealing technology and retention of hermeticity at the joint section are recognized as critical feasibility issues [5]. In addition to joint processing, degradation of mechanical properties as a result of neutron irradiation is a concern and a technical hurdle for nuclear structural applications in general [6,7].

Previous studies investigated the effects of neutron irradiation on the torsional shear strength of various SiC-to-SiC joints fabricated by solid state diffusion bonding using titanium (Ti) and molybdenum (Mo) interlayers, glass ceramic joining, reaction sintering with a Ti-Si-C system, liquid-phase sintering (LPS) SiC joining, and hybrid processing of polymer pyrolysis and chemical vapor infiltration [8,9]. Most of these joining concepts were originally developed for non-nuclear applications.

The irradiation temperatures and displacement damage levels projected for SiC applications range from 300 to 800°C and 2–9 displacements per atom (dpa), respectively. Post-irradiation mechanical tests found that all the joints retained a torsional shear strength exceeding 80 MPa. These positive results encouraged further investigation of these joints for nuclear applications. Since the radiation damage levels were low compared with the total damage expected in nuclear fusion and advanced fission reactors [10], this study investigated high-dose neutron irradiation effects on selected joints previously studied.

The other focus of the irradiation experiments in this study is investigation of SiC joints, previously little studied for nuclear applications. The joining methods include spark plasma sintering (SPS), pressureless reaction sintering with a Ti-Si-C system, and low-pressure LPS of cold-pressed SiC green body (low-pressure LPS + CP hereafter). Joining SiC to SiC by SPS has been actively developed in recent years. The rapid heating (>50°C/min) and short dwell time (~5 min) of the SPS process enabled the formation of a unique microstructure in the bonding layer, not seen in joints fabricated by conventional hot-pressing [11–14]. Since Ti-diffusion-bonded SiC retained its strength after irradiation in a previous study [8], a Ti interlayer was also applied using the SPS process in this study. For the pressureless Ti-Si-C reaction sintering process, a pressureless joining process was recently demonstrated [9], contrasting to the 30–40 MPa applied stress in a previous study [8]. In addition, a preliminary irradiation study found insignificant changes in joint strength following irradiation at 290°C to 8.7 dpa [9]. This joint is further investigated in this study, as the pressureless joining process is promising for the integration of large, complex-shaped components. Low-pressure LPS of cold-pressed SiC green body processing is also a process that uses reduced pressures of ~0.1 MPa applied during heating in contrast to the applied stress of 20 MPa used for previously fabricated joints [8]. Low-pressure sintering represents important progress toward fully pressureless LPS SiC joining.

Studying neutron irradiation effects on SiC joints requires a reliable mechanical test method applicable to a miniature test specimen because of the limited volume of irradiation capsules (e.g. 50×6×6 mm^3 in this study). Previous efforts in the development of miniature specimen testing techniques established the validity of torsional shear testing of hourglass ceramic joints [15,16]. The advantages of torsion testing over existing test methods such as single-lap offset

tests (ASTM D905–08) and asymmetrical four-point bending tests (ASTM C1469–10) include small test specimen size (6×6×3 mm^3), pure shear failure of specimens achieved for certain joint types, and a uniform stress state at the outer surface of the bonding layer in the torsion specimen. ASTM standardization of the torsional shear test is in progress. Detailed comparisons of joint strength test methods can be found elsewhere [8]. The torsional shear test was also employed in this study so that the joint strengths could be compared to previous irradiation studies.

2. Experimental

2.1 Processing of SiC joints

The bonding phases tested include calcia-alumina (CA) glass ceramic, LPS SiC, and Ti_3SiC_2 MAX phase–based ceramics. Chemical-vapor-deposited (CVD) β-SiC (Dow Chemical Co., Marlborough, Massachusetts) with purity >99.9995% was the substrate material for all the joints.

Pressureless CA glass ceramic joining was applied in the same manner as used in previous irradiation experiments [8]. A CVD SiC plate was machined to form half-pieces of a miniature hourglass in advance of the joining. The feedstock of the bonding layer was 49.7 wt % CaO and 50.3 wt% Al_2O_3 powders, heated in a Pt crucible at 1650° in air for 1 h, to obtain a glass-ceramic by melt-quenching and applied as ethanol based slurry on both hourglass half-pieces. The samples were joined by heating in a tubular oven under an argon flow for 10 min at 1480°C in the absence of applied pressure [15]. The joint phases of the CA glass ceramic were reported to be a mixture of calcium aluminum oxides such as $3CaO{\cdot}Al_2O_3$ and $12CaO{\cdot}7Al_2O_3$ [15].

Three types of LPS-SiC joints were fabricated: pressure-assisted LPS-SiC nanopowder using slurry or using green sheet, and low-pressure LPS-SiC nanopowder with cold-pressing. They are referred to as pressure-assisted LPS-SiC (slurry), pressure-assisted LPS-SiC (green sheet), and low-pressure LPS-SiC with CP, respectively. The processing conditions for the pressure-assisted LPS-SiC (slurry and green sheet) joints can be found elsewhere [9]. The green sheet consisted of the feedstocks for the SiC nanopowder slurry plus an organic binder to give the sheet enough strength and flexibility for handling. The thickness of the bonding layer was easily adjusted by adjusting the green sheet thickness. However, the organic additives in the sheet affected the quality of the final product. In contrast, the slurry method did not require organic additives. It achieved a higher-purity feedstock system. The drawback of the slurry method was the difficulty of controlling the joint thickness. The slurry was prepared by milling a mixed powder with zirconia balls in ethanol. The mixed powder consisted of a SiC nanosize powder (average diameter ~30 nm, Nanomakers, France), an Al_2O_3 powder (average diameter ~0.3 mm, Kojundo Chemical Lab. Co., Japan), and a Y_2O_3 powder (average diameter ~0.4 mm, Kojundo Chemical Lab. Co., Japan). The total amount of oxide additives was 6 wt% with a weight ratio of Al_2O_3:Y_2O_3 = 3:2. The slurry was sandwiched between CVD SiC plates and then dried at 80°C before heating. The joint was then formed by hot-pressing at 1850°C for 1 h in an argon atmosphere, under a pressure of 10 MPa. The feedstock for the green sheet was the same as that for the slurry sintered joint, except for the additional use of organic binders. The green sheet was provided by Gunze Ltd. in Japan. SiC/green sheet/SiC sandwiches were joined by hot-pressing, with the same hot-pressing conditions as for the slurry joint. The dimensions of the SiC substrate were 40×40×5mm. The joint formed by low-pressure LPS-SiC with CP was also fabricated using a powder mixture consisting of the Nanomakers SiC nanopowder and sintering additives, Al_2O_3

powder (Nano Products Corp.), and Y_2O_3 powder (Nanostructured and Amorphous Materials), with a weight ratio of Al_2O_3:Y_2O_3 = 3:2, with organic agents. The total amounts of oxide additives and organic agents were 6 and 3.5 wt%, respectively. The feedstock powders were mixed by ball milling with a silicon nitride media. The joints were formed by sandwiching a dried mixed powder between CVD SiC plates followed by cold-pressing at 10 MPa in a graphite die for green powder compaction. The size of the CVD SiC substrate was 21×31×6 mm. The sandwiched materials were heat-treated at 1875°C for 1 h in a flowing argon atmosphere in a graphite die. A very small pressure (~0.1 MPa) was applied during heating to hold the specimen in the furnace. All bonded plates were machined into miniature hourglass specimens for irradiation.

Four types of SiC joints with a Ti_3SiC_2 MAX phase–based bonding layer were fabricated: hot-pressed MAX-phase joint, pressureless MAX-phase joint, SPS MAX-phase joint, and Ti diffusion bond. The processing recipe for hot-pressed MAX-phase–bonded SiC has been reported [17]. A tapecast mixture of TiC and Si powders in a 3:2 ratio with an organic binder was used as the bonding layer. This powder mixture exhibited a displacement reaction of 3TiC + 2Si -> Ti_3SiC_2 + SiC during heating. Joining was accomplished by heating the specimens at approximately 20°C/min with a 4 h hold at 1425–1435°C and a 20°C/min cool-down. A pressure of 40 MPa was maintained during the 24 h hold. The joint thickness of 15 μm was controlled by the thickness of the tape casting. For fabrication of the pressureless MAX-phase bond, a set of joining agent materials were purchased from Hyper-Therm High Temperature Composites (currently Rolls-Royce High Temperature Composites, Huntington Beach, CA). The Ti-Si-C phase-based joints of CVD SiC were produced based on a pressureless slurry process following the Hyper-Therm formula. Note that no pressure was applied during the formation of the joints in a furnace. The bonded plates were machined into hourglass torsion specimens. Details of the raw materials and the process conditions are proprietary. The SPS MAX-phase joints were fabricated using a 25 μm Ti foil. As in the CA glass joint processing, pre-machined half-pieces of CVD SiC substrate were used for joining. The samples were loaded in the SPS equipment (FCT HP D 25, FCT Systeme GmbH) in a cylindrical graphite mold and heated under pulsed current at a rate of 50°C/min with a dwell time of 5 min at 1700°C under a vacuum of 5 Pa. The optimized pressure was 50 MPa. Details of the process development can be found elsewhere [18]. The processing recipe for the Ti diffusion bond has been reported [9]. A Ti foil (25 μm thick, 99.94% pure, Alfa-Aesar, Ward Hill, MA) was used as the interlayer. The SiC/Ti foil/SiC sandwiches were joined by hot-pressing at 1500°C with heating rate of 10°C/min for 1 h in vacuum, under a uniaxial pressure of 17 MPa. Titanium powder was used as a getter to reduce the oxygen partial pressure in the furnace

Table 1 Summary of test materials, processing conditions, irradiation conditions, and joint strengths. The parentheses indicate the standard deviation. The fracture appearance after torsion testing is also indicated by S (substrate failure), J (joint failure), or J/S (failure at both substrate and joint).

Joining type	Specimen type	Processing conditions	Bonding layer	Neck diameter of hourglass	Test conditions	Torsional strength [MPa]	Number of torsion tests	Fracture surface
Glass ceramic based joining	Pressureless CA glass ceramic	1480°C 10 min 0 MPa	$12CaO \cdot 7Al_2O_3$, $3CaO \cdot Al_2O_3$	5	Unirradiated 530° C/20.2dpa 780° C/2.3dpa	104 (26) 88 (48) 110 (10)	10 3 3	J and J/S J/S J and J/S
LPS SiC base joining	Pressure-assisted LPS-SiC (slurry)	1850°C 1 h 10 MPa	SiC, Y-Al-Zr oxides	4	Unirradiated 530° C/20.2dpa 730° C/2.3dpa	319 (31) 319 (37) 25 (44)	6 3 3	S S S and J
	Pressure-assisted LPS-SiC (green sheet)	1850°C 1 h 10 MPa	SiC, Y-Al-Zr oxides	4	Unirradiated 530° C/20.2dpa 730° C/2.3dpa	116 (24) 130 (32) 44 (88)	9 3 4	S and J/S S J
	Low-pressure LPS of cold pressed SiC green body	1875°C 1 h 0.1 MPa at 1875°C 10 MPa at RT	SiC, Y-Al oxides	4	Unirradiated 480° C/2.9dpa 730° C/2.3dpa	114 (21) 146 (32) 126 (37)	9 4 3	S S S
MAX phase forming joining	Hot-pressed MAX-phase joint	~1430°C 4 h 40 MPa	Ti_3SiC_2, SiC	5	Unirradiated 530° C/20.2dpa	112 (38) 108 (12)	6 3	S and J J/S
	Pressureless MAX phase	Proprietary for temperature and holding time 0 MPa	Ti_3SiC_2, SiC, TiC	5	Unirradiated 490° C/2.9dpa 780° C/2.3dpa	147 (12) 110 (19) 107 (19)	8 4 3	S S S
	SPS MAX phase	1700°C 5 min 50 MPa	Ti_3SiC_2, SiC	5	Unirradiated 510° C/2.9dpa	82 (17) 73 (47)	4 3	S S, J, and S/J
	Ti diffusion bond	1500°C 1 h 17 MPa	Ti_3SiC_2, $TiSi_2$	5	Unirradiated 510° C/2.9dpa 780° C/2.3dpa	133 (22) 179 (7) 161 (3)	6 3 3	S S S

The geometry and appearance of the hourglass joint specimens are shown in Fig. 1. The dimensions of the test specimen were 6 ×6 ×3 mm, projecting as a 6 mm square when viewed normal to the bond plane (Fig. 1a). The square section was 1 mm thick, and the bonding layer was located at the midplane of the specimen in the 2.9–3.0 mm total thickness direction (Fig. 1a–c). The neck diameter of the hourglass specimen was 4 mm for the LPS-SiC–based joints (Fig. 1c) and 5 mm for the other joints (Fig. 1b). The neck diameter was chosen to enable comparison with previous work.

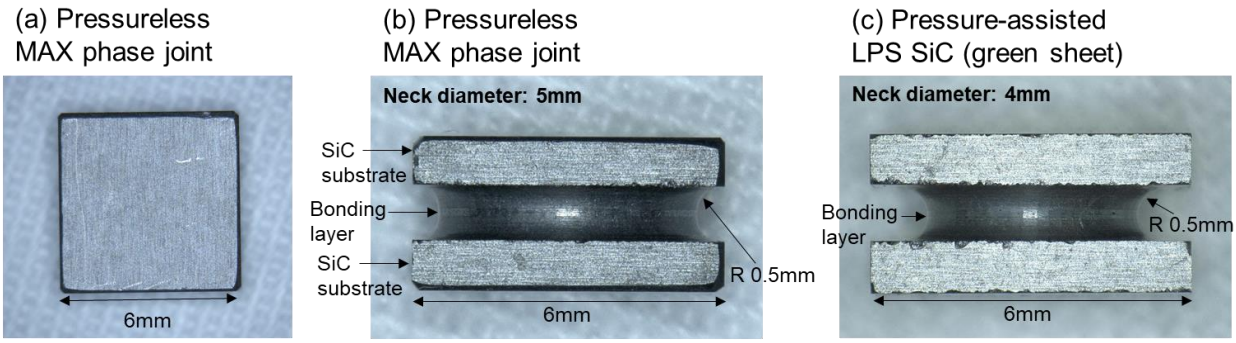

Fig. 1. Geometry of the hourglass SiC joint specimens: (a) top view and (b) side view of pressureless MAX-phase joint and (c) side view of pressure-assisted LPS-SiC (green sheet) joint.

2.1 Irradiation and post-irradiation examination

The joint specimens were neutron irradiated at 480–780°C to 2.3–20.2×10^{25} n/m^2 (E >0.1 MeV) in target rod rabbit holders position (position TRRH 5 or 7) in the High Flux Isotope Reactor at Oak Ridge National Laboratory. Each rabbit capsule contained 16 hourglass-shaped specimens. Temperature was controlled by varying the size of the gas gap between the holder and the housing. Thermal analysis using an ANSYS finite element software package was conducted to ensure that the specimens would be irradiated at the desired temperatures. The fluence corresponded to 2.3–20 dpa-SiC, assuming equivalence of 1 dpa = 1×10^{25} n/m^2 (E >0.1 MeV). This paper consistently uses the displacement damage for the SiC substrate rather than the bonding layer. Irradiation temperatures were determined by post-irradiation measurement of the length change of passive SiC temperature monitors using a NETZSCH DIL 402CD dilatometer as swelling of SiC starts recover at irradiation temperature [19]. The temperature monitors were designed to physically contact the substrates of the joint specimens during irradiation. The irradiation conditions are summarized in Table 1. Pressureless CA glass ceramic, pressure-assisted LPS-SiC (slurry and green sheet), and hot-pressed MAX-phase were irradiated to a neutron damage of 20 dpa. The other joints were irradiated to 2.3–2.9 dpa. The total duration of the irradiation was ~350 days for 20 dpa and ~25 days for 2.3–2.9 dpa. There was a reactor shutdown approximately every 25 days during the longer irradiation.

Torsion testing was conducted to evaluate the shear strength of the joints using a TestResources 160 GT–125Nm torsion system with pairs of flexible couplers and sample grips. The flexible coupling maintains the alignment during loading. Aluminum-alloy tabs were installed at the square grip sections to obtain uniform grip stress distributions. Details of the torsion test system have been reported [9]. The rotation speed during test was 0.15 degree/min. Nominal shear strength values (τ) are given by the following equation

$$\tau = 16Tk/\pi d^3 , \qquad (1)$$

where T is the applied torque, d is the specimen diameter of the neck, and k is the stress concentration factor due to the fillet notch, based on ASTM Standard F734-95. This study adopted k = 1 to compare with the results from the previous study. Since k depends on the diameter of the hourglass specimen, the strength is comparable only when the specimen geometry is the same. The number of torsion tests is shown in Table 1. All the tests were

conducted at ambient temperature, approximately 23°C. Torsion shear testing can provide the shear strength based on Eq. (1) if the specimen fails in shear and a fracture initiates from the surface of the neck section. However, only a limited number of joints exhibited a shear failure. As in the previous studies [8,9], the specimen fracture appearance was categorized as one of three types: joint failure (J), substrate failure (S), and failure at both substrate and joint (S/J) (Fig. 2). Even for joint failure, the fracture initiation site could not be identified from the fracture surface. Therefore, the strength measured was the torsional strength rather than shear strength. Furthermore, the strength should be carefully compared among the specimens joined before and after machining as the machining processes affect surface condition. However, the data are still useful for comparing the strength of the joints before and after irradiation.

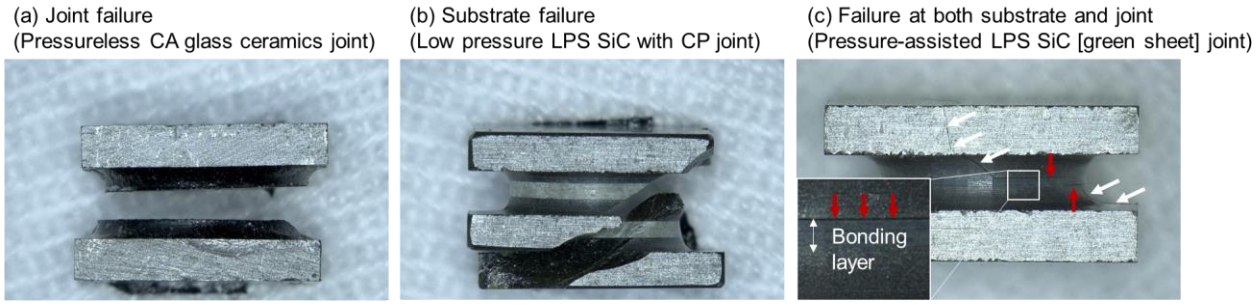

Fig. 2. Examples of fracture appearance of SiC joints subject to torsion test: (a) joint failure, (b) substrate failure, and (c) failure at both substrate and joint. White and red arrows in image (c) indicate cracks within the substrate and along the joint interface, respectively.

The fracture appearance of the joint specimens was examined using a KEYENCE VHX-1000 digital microscope. Scanning electron microscopy (SEM) and focused ion beam (FIB) milling on a FEI Versa 3D DualBeam were also used. Cross sections of the joint specimens that had not experienced mechanical testing were imaged using SEM. Specimen preparation for analysis of the cross section was performed using mechanical polishing with diamond films followed by final polishing with a colloidal silica suspension. Electron backscatter diffraction (EBSD) analysis used an Oxford Instruments Nordlys II detector on the Versa SEM. The results of EBSD analysis were presented only for pre-irradiation specimens because of the low data quality (degradation of Kikuchi pattern quality) of irradiated specimens attributed to radiation-induced lattice disordering [9]. Thin foils for transmission electron microscopy (TEM) observation were prepared using the FIB operated at 30 kV for rough milling and 2 and 5 kV for final thinning, followed by low-energy ion milling using a Fischione Model 1040 NanoMill operated at 600 and 900 eV. TEM observations were conducted using a JEOL JEM2100F with TEM and scanning TEM (STEM) modes operated at 200 kV.

3. Results

3.1 Low-dose neutron irradiation of LPS SiC-based joints

Cross sections of the as-fabricated LPS-SiC–based joints are shown in Fig. 3. The joint thickness of the pressure-assisted LPS-SiC (slurry) was about 100 μm and the bonding layer was highly dense (Fig. 3a). In addition, no macroscopic cracks or interface debonding were found.

The green sheet joint had a thicker bonding layer (150 μm). The microstructure was inhomogeneous even in the cross-section of the same specimen, with localized ~100 μm pores (Fig. 3b). The joint fabricated by low-pressure LPS-SiC with CP exhibited micropores within a 400–500 μm joint thickness. The bonding layer contains some amount of porosity (<5μm in size). It was expected that full densification of the bonding layer would require a higher cold pressure on the SiC powder compact (e.g., 100 MPa) to achieve high green density, based on a previous study of an LPS-SiC monolith [20]. LPS-SiC–based joints are known to contain SiC grains and secondary phases attributed to alumina and yttria sintering additives. These oxides are known to promote sintering by the formation of a eutectic liquid that acts as a mass transfer medium during sintering [21]. The oxide secondary phases in the LPS-SiC–based joints were examined using SEM-EDS (energy-dispersive x-ray spectroscopy) analysis as shown in Fig. 4. Yttrium, aluminum, and oxygen, which were in the sintering additives, were clearly detected as elements of secondary phases in three types of joints. In addition, the secondary phases contained zirconium impurity in both types of pressure-assisted LPS-SiC joints. The Zr likely came from the ball milling media used during processing. Zirconium was not detected in the low-pressure LPS-SiC with CP joint because a zirconium-free media was used. The LPS-SiC green sheet joint had significant local segregation of the oxide phases. In contrast, the other two joints showed broader dispersion of the oxide phases within the bonding layer. The chemical compositions of the oxide phases in both types of pressure-assisted LPS-SiC joints varied at different locations, revealing nonuniformity in the joint microstructures. The low-pressure LPS-SiC with CP showed better consistency of the joint microstructure. A Y-Al oxide was a dominant secondary phase at different locations analyzed.

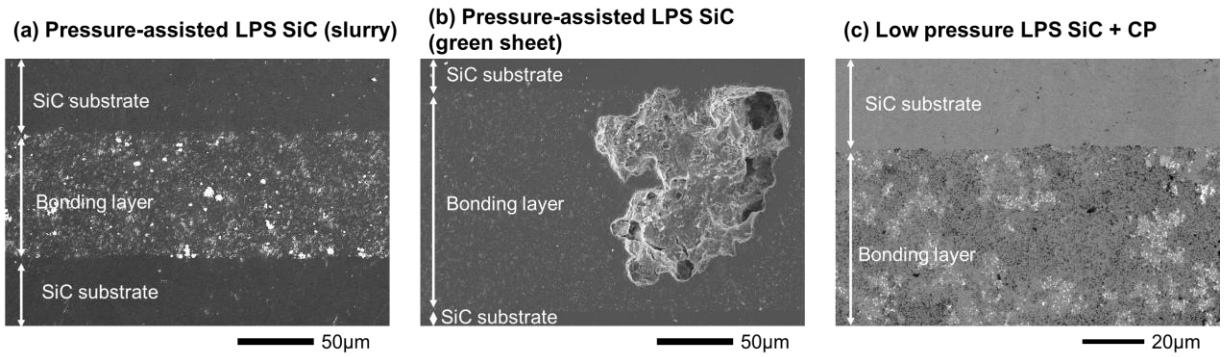

Fig. 3. Secondary electron micrographs of sections through unirradiated LPS-SiC–based joints: (a) pressure-assisted LPS-SiC (slurry), (b) pressure-assisted LPS-SiC (green sheet), and (c) low-pressure (~0.1 MPa) LPS-SiC with CP.

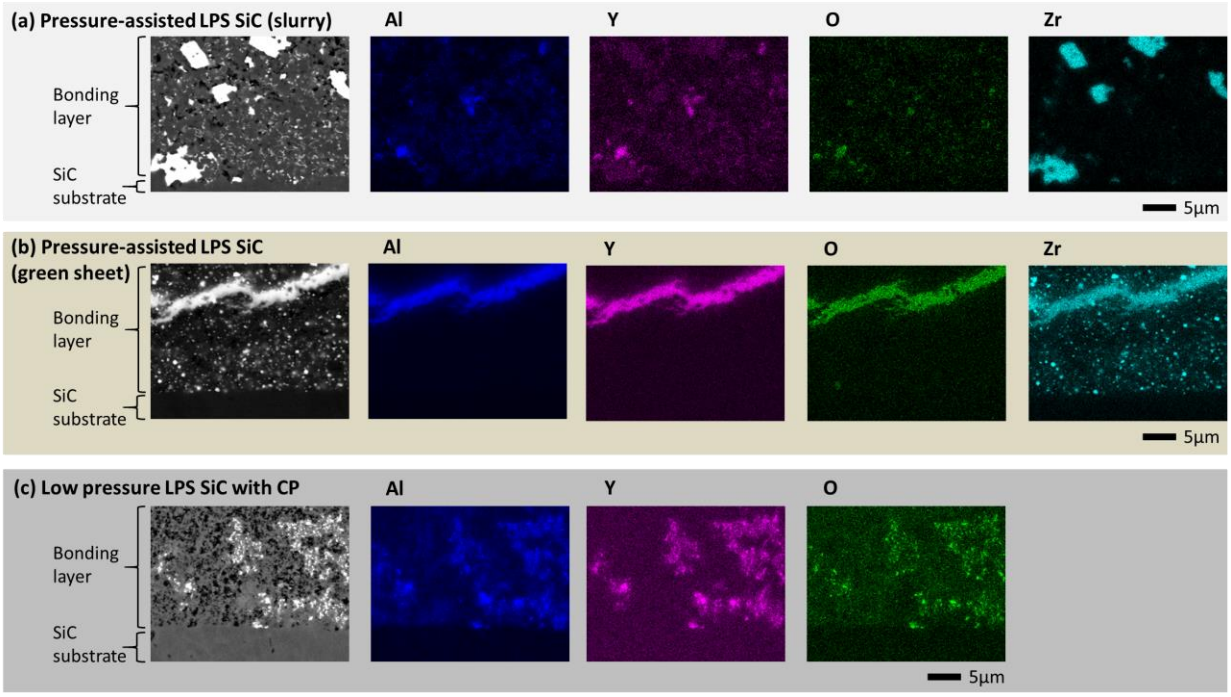

Fig. 4. Backscatter electron micrographs and EDS elemental maps of as-fabricated LPS-SiC–based joints.

Fig. 5 shows the torsional strengths of the unirradiated and irradiated SiC joints. The pressure-assisted LPS-SiC green sheet joint and low-pressure LPS-SiC with CP joint showed torsional strengths of ~115 MPa in an unirradiated condition. The LPS-SiC slurry joint showed exceptionally high torsional strength of 319 MPa before irradiation. It should be noted that there are various factors potentially affecting the torsional strength, including strength of the bonding layer, interfacial bonding strength, joint thickness and modulus, residual stress, and surface condition after machining. The fracture appearance of the joint is a useful indication of the robustness of the joint layer and the interface [8]. Substrate fracture surface can be seen in robust joints. The crack could initiate either within or out of the bonding layer because of load sharing between the joining region and substrate and the probabilistic nature of fracture in ceramics [16]. Fracture surface of the joint plane indicates that the bonding layer or joint interface is relatively weak. Fracture surface of both joint and substrate implies intermediate strength of the joint layer and interface. That explanation was also applicable in this study: the fracture surfaces of the LPS-SiC slurry joint and the low-pressure LPS-SiC joint were always in the substrate, because their bonding layers were dense and the substrate and LPS-SiC were well bonded. The LPS-SiC green sheet joint failed at the substrate or substrate/joint mixture because of large pores.

Irradiation at 730°C to 2.3 dpa significantly degraded both types of pressure-assisted LPS-SiC joints (slurry and green sheet). Two of the four slurry joints and three of the four green sheet joints were debonded when the specimens were removed from the irradiation vehicle, as shown in Fig. 6. The failures occurred at the joint interfaces. There was no indication of mechanical damage during disassembly of the radiation vehicle, and the other joint specimens were intact. Joint strengths of the irradiated joints are also shown in Fig. 5. The strengths of the failed specimens were considered to be near zero. Since a majority of the specimens failed before testing, the strengths after irradiation were significantly lower than the unirradiated values. The

low-pressure LPS-SiC with CP joint retained its joint strength, with substrate fracture surfaces following neutron irradiation at 480°C to 2.9 dpa and 730°C to 2.3 dpa, as shown in Fig. 5. Cross-sectional SEM observation (Fig. 7) did not find any microstructural changes, such as interfacial debonding and cracking, as the result of neutron irradiation, which explains the strength retention following irradiation.

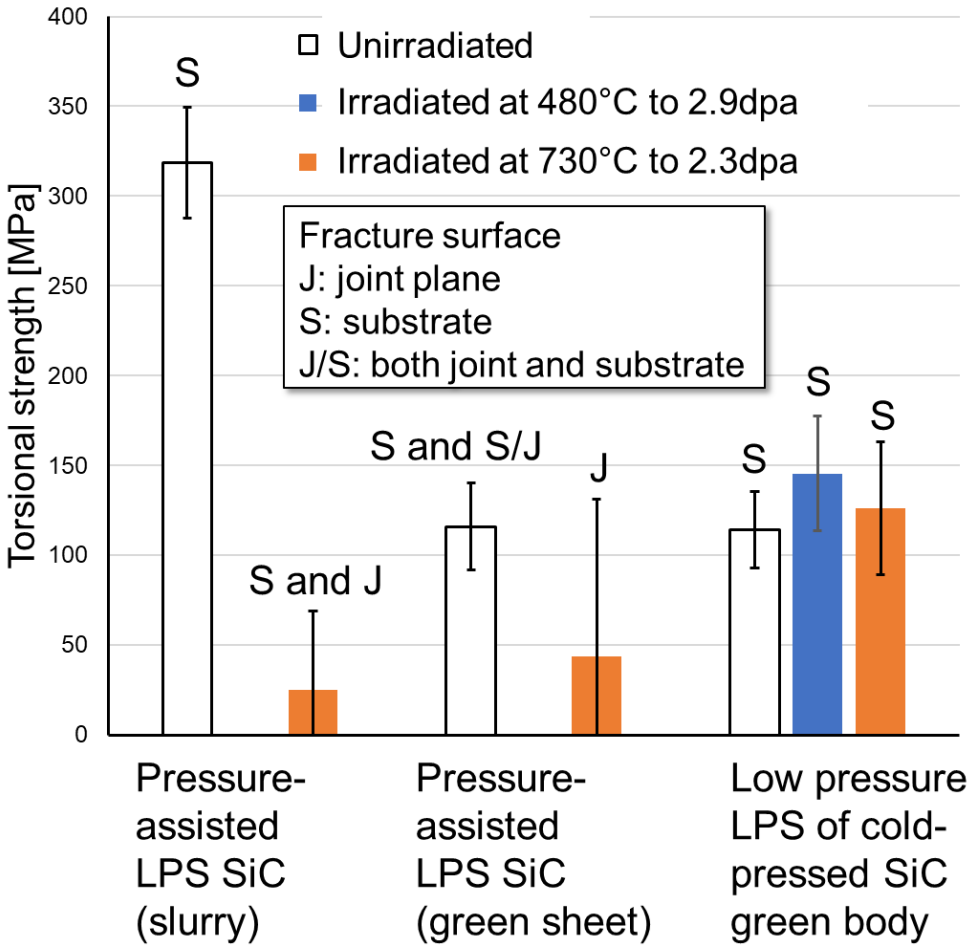

Fig. 5. Torsional strengths of unirradiated and neutron-irradiated LPS-SiC–based joints. Appearance of fracture surface is also indicated.

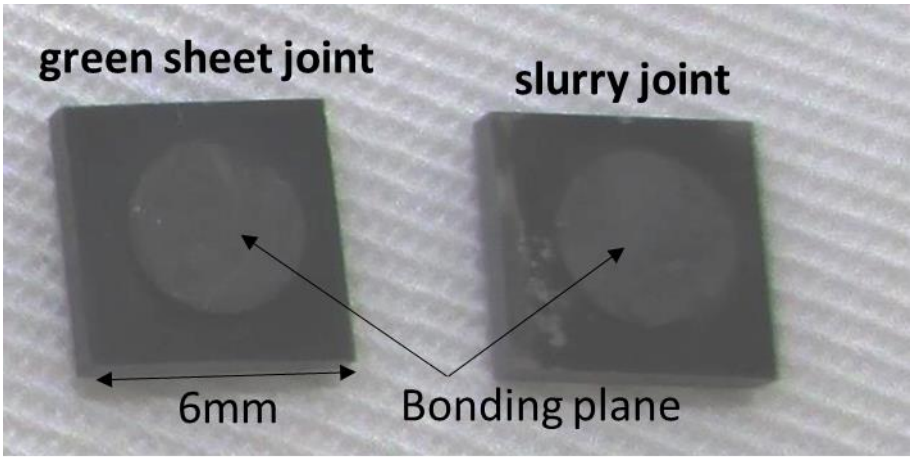

Fig. 6. Half-pieces of pressure-assisted LPS-SiC (slurry and green sheet) joints following irradiation at 730°C to 2.3 dpa, showing failure at the joint plane during irradiation experiment. See fractography of unirradiated sample in Fig. 2c for comparison.

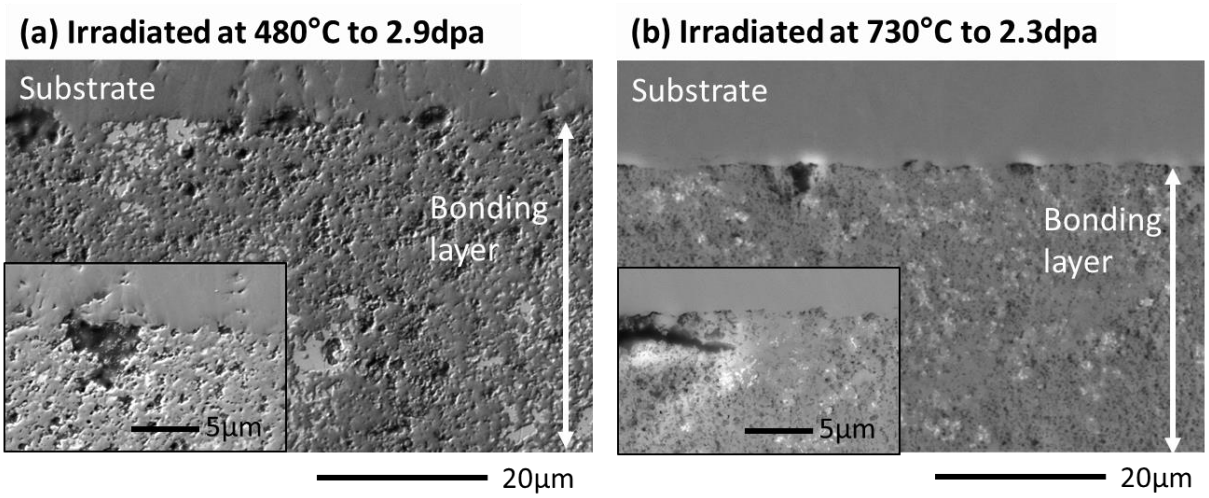

Fig. 7. Secondary electron micrographs of SiC joints fabricated by low-pressure LPS of cold-pressed SiC green body: (a) irradiated at 480°C to 2.9 dpa, and (b) irradiated at 730°C to 2.3 dpa.

3.2 Low-dose neutron irradiation of MAX phase–based joints

Phases in unirradiated specimens of the Ti diffusion bond, pressureless MAX-phase joint, and SPS MAX-phase joint were analyzed by EBSD (Fig. 8). All the joints contained a Ti_3SiC_2 MAX phase as a main joint phase. The Ti diffusion bond had a Ti_3SiC_2 phase near the joint interface and a mixed structure of Ti_3SiC_2 and $TiSi_2$ at the center of the joint layer [9] (Fig. 8a). A mixture of Ti_3SiC_2 and Ti silicide was also reported in Ti diffusion-bonded SiC [22]. The phase map of the pressureless MAX-phase joint shows that the dominant joint phases were Ti_3SiC_2 and SiC (mainly 6H or 4H hexagonal structure) and the minor phase was TiC (Fig. 8b). The EBSD result was qualitatively consistent with the EDS results, despite a possible mistake in

the assignment of phases between TiC and 3C SiC in the EBSD software because of a similar Kikuchi pattern. The SPS MAX-phase joint had a dominant Ti_3SiC_2 phase (~90%) in the bonding layer in addition to a minor TiC phase near the middle of the bonding layer (Fig. 8c). Note that 3C SiC grains within the bonding layer were likely an artifact, as was confirmed by EDS analysis. A combination of Ti_3SiC_2 and TiC phases was also reported for hot-pressed Ti diffusion-bonded SiC [23]. No notable grain texture was found for the MAX phase–based joints except for a $TiSi_2$ phase in the Ti diffusion bond. All three types of joints developed some cracks during processing, likely due to a mismatched coefficient of thermal expansion between SiC and the joint phases. Cracking in the Ti diffusion bond was very minor and was not obvious under low–magnification SEM observation. The pressureless MAX-phase joint contained cracks across the bonding layer. Cracks in the SPS joint also propagated approximately perpendicular to the joint interface. The crack paths in the SPS MAX-phase joint followed grain boundaries, based on comparison of the SEM image and the EBSD map.

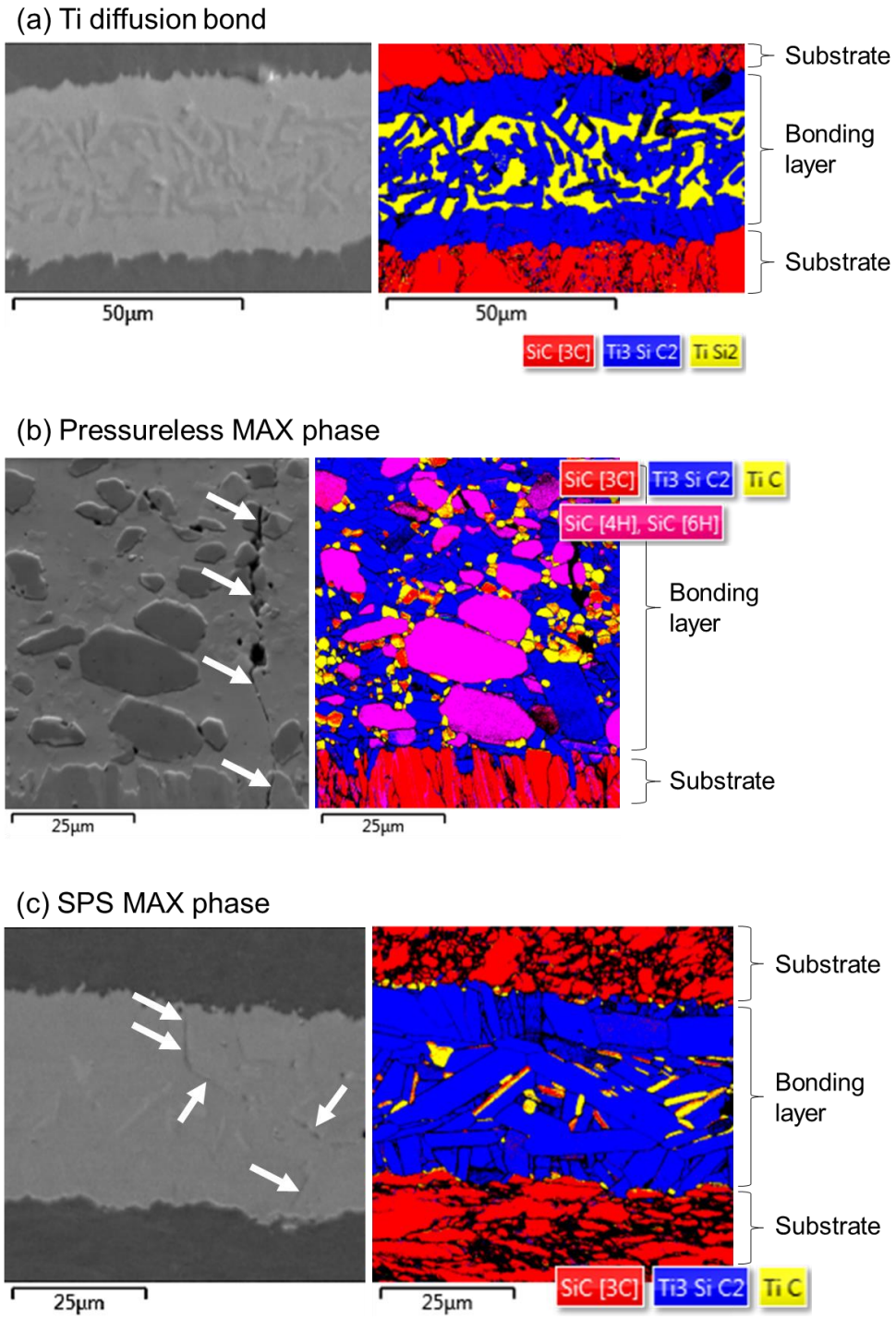

Fig. 8 SEM micrographs and EBSD phase maps of three types of unirradiated SiC joints containing Ti_3SiC_2 MAX phase as a main joint phase: (a) Ti diffusion bond, (b) pressureless MAX-phase joint, and (c) SPS MAX-phase joint. Cracks are noted by arrows in the micrographs.

Fig. 9 and Table 1 summarize the results of the torsional shear tests of the unirradiated and irradiated SiC joints. All the MAX phase–based joints failed at the SiC substrate regardless of irradiation, implying that the joints were robust. The average torsional strengths of the Ti

diffusion bond, pressureless MAX-phase joint, and SPS MAX-phase joint were 133, 147, and 82 MPa before irradiation, respectively. The strengths were not significantly degraded by irradiation at 490–510°C to 2.9 dpa or irradiation at 730–780°C to 2.3 dpa. The most significant change was for the pressureless MAX-phase joint irradiated at ~500°C, which showed a ~25% reduction in torsional strength. However, the torsional strength remained high (>100 MPa) and the failure location was the substrate. Hence, it is reasonable to conclude that MAX phase–based joints with different microstructures were resistant to irradiation in terms of maintaining strength. This similarity may be associated with all the MAX phase-based joints having the Ti_3SiC_2 phase facing the SiC substrate. Contrary to the high torsional strength after irradiation, cross-section SEM observation found radiation-induced damage. Cracks propagating perpendicular to the joint interface were found in the Ti diffusion bond (Fig. 10a); they were absent before irradiation. The pressureless MAX-phase joint also experienced cracking during irradiation; the crack density clearly increased from the unirradiated to the irradiated condition (Fig. 10b). These two types of irradiated joints showed similar microcracking behavior at ~500 and ~750°C. In the SPS MAX-phase joint, process-induced cracks opened up during irradiation, as shown in Fig. 10c. Even though irradiation-induced damage was found, not all of the irradiated joints showed interfacial debonding, which is one explanation for why the joint did not fail at the interface or within the bonding layer during torsion tests.

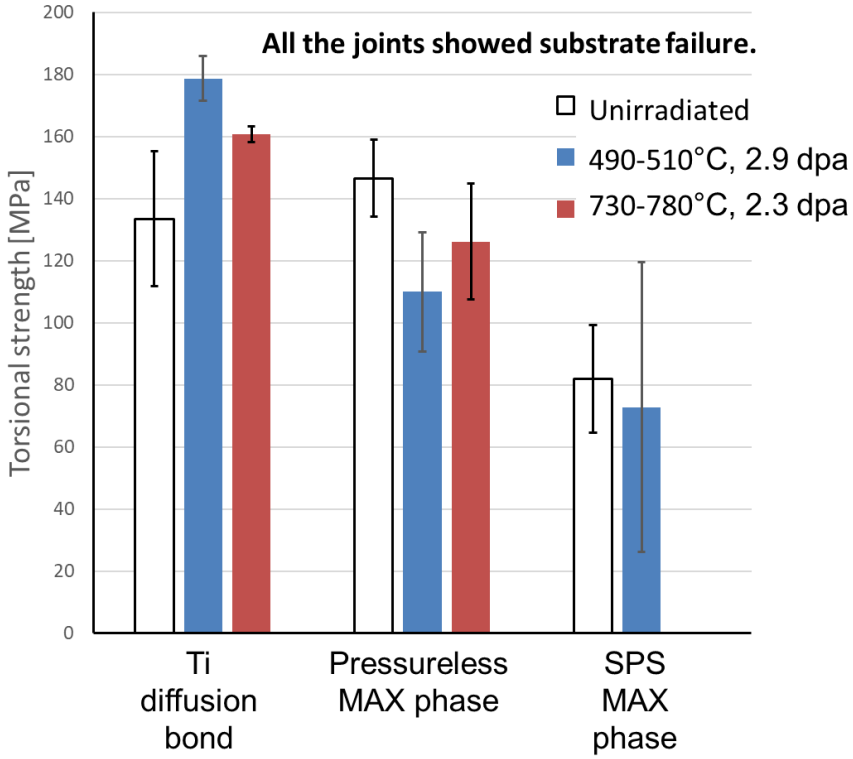

Fig. 9 Torsional strength of MAX phase–based joints before and after irradiation. All the joints failed at the substrate regardless of irradiation.

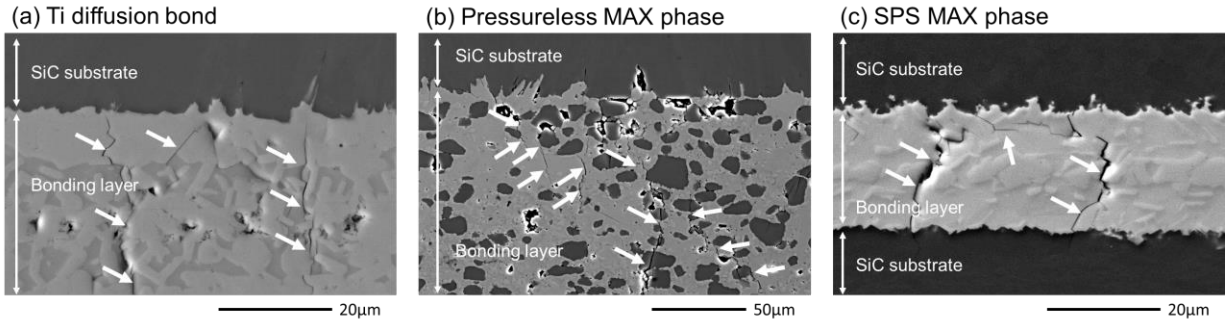

Fig. 10 Cross-section SEM micrographs of MAX phase–based joints following neutron irradiation at 490–510°C to 2.9 dpa: (a) Ti diffusion bond, (b) pressureless MAX-phase joint, and (c) SPS MAX-phase joint.

3.3 High-dose neutron irradiation of selected joints

The pressure-assisted LPS-SiC joints (both slurry and green sheet joints), pressureless CA glass ceramic joint, and hot-pressed MAX-phase joint were evaluated before and after neutron irradiation at 530°C to 20 dpa. To the best of our knowledge, this is the highest level of neutron damage reached in testing ceramic joints for nuclear applications. The microstructures of the as-fabricated LPS-SiC joints were shown in Fig. 3 and Fig. 4. The joint phase of the pressureless CA glass ceramic joint was found to be a mixture of $3CaO{\cdot}Al_2O_3$ and $12CaO{\cdot}7Al_2O_3$, according to detailed evaluation using XRD and TEM [24]. The hot-pressed MAX-phase joint had a mixture of phases (Ti_3SiC_2 and 3C SiC) as reported [8]. This microstructure was expected based on the displacement reaction of $3TiC + 2Si = Ti_3SiC_2 + SiC$.

The torsional strengths of the unirradiated and irradiated joints and the fracture appearance are shown in Fig. 11 and Table 1. The pressureless CA glass ceramics joint, pressure-assisted LPS-SiC green sheet joint, and hot-pressed MAX-phase joint showed torsional strengths of ~100 MPa in the unirradiated condition, which is consistent with previous results [8]. The fracture surface varied among different test specimens. The pressureless CA glass ceramic joint exhibited fracture surface of the joint plane or both the substrate and the joint. The MAX-phase joint showed fracture at the substrate or the joint plane. Surprisingly, the high-dose neutron irradiation caused no notable strength degradation for any of the joints investigated, shown in Fig. 11. Although the pressureless CA glass ceramic joint and hot-pressed MAX–phase joint showed a reduction in torsional strength after irradiation, the effect of irradiation was insignificant considering the standard deviation. The observation of the fracture surfaces also supported the results of the torsion testing; none of the joints showed signs of strength degradation, such as a change in the fracture surface from substrate to joint, or from failure at the joint/substrate interface to failure only at the joint. This demonstrates that those four types of SiC joints survived the high-dose neutron irradiation.

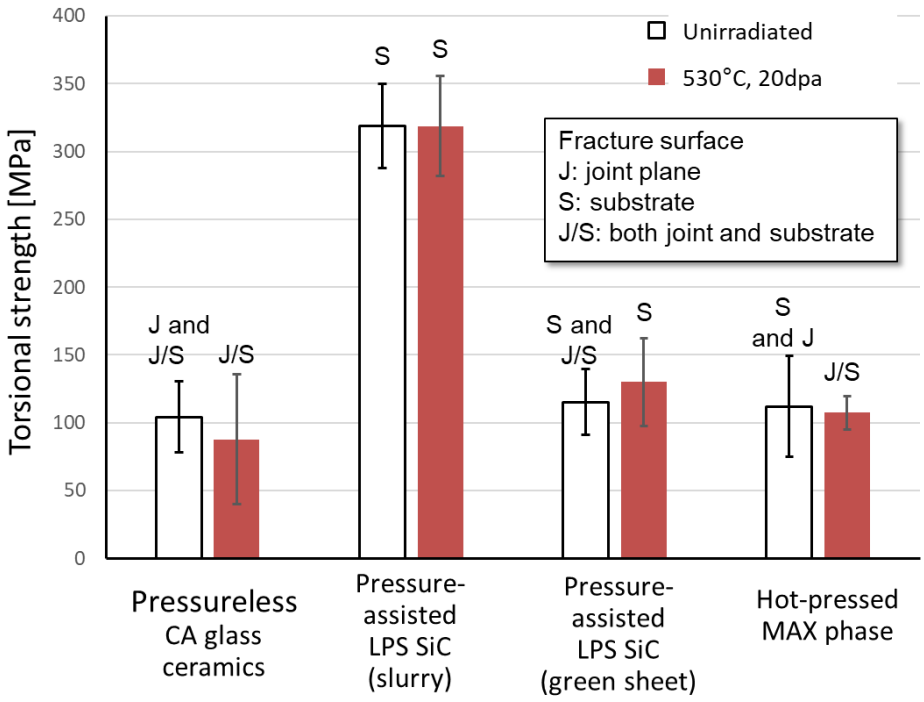

Fig. 11 Torsional strength of SiC joints irradiated at 530°C to 20 dpa-SiC. Error bars indicate one standard deviation. The appearance of fracture surfaces is also indicated.

Fig. 12 shows backscattered electron (BSE) SEM images of polished cross-sections of the pressureless CA glass ceramic joint before and after irradiation. The joint contained two major phases, $3CaO{\cdot}Al_2O_3$ and $12CaO{\cdot}7Al_2O_3$ [24], which were distinguished based on image contrast. The joint thickness was ~10 μm, and it varied (5–15 μm) among different specimens because the joints were individually made. The joint thickness stayed within this range following irradiation. The as-fabricated joint contained cracks propagating approximately perpendicular to the joint interface. The crack spacing ranged from ~10 to ~20 μm, and it was similar following irradiation. Neither unirradiated nor irradiated joints showed any interfacial debonding. Hence, the joint did not show notable microstructural changes from irradiation in SEM images. Fig. 13 shows cross-section BSE micrographs of the pressure-assisted LPS SiC (slurry and green sheet) joints after irradiation. No notable microstructural features were found, and no irradiation-induced cracking or debonding. The distribution of the oxide phases in the green sheet joint was different among the reference and irradiated specimens, based on a comparison of Fig. 4 and Fig. 13, indicating nonuniform joint microstructure among different specimens.

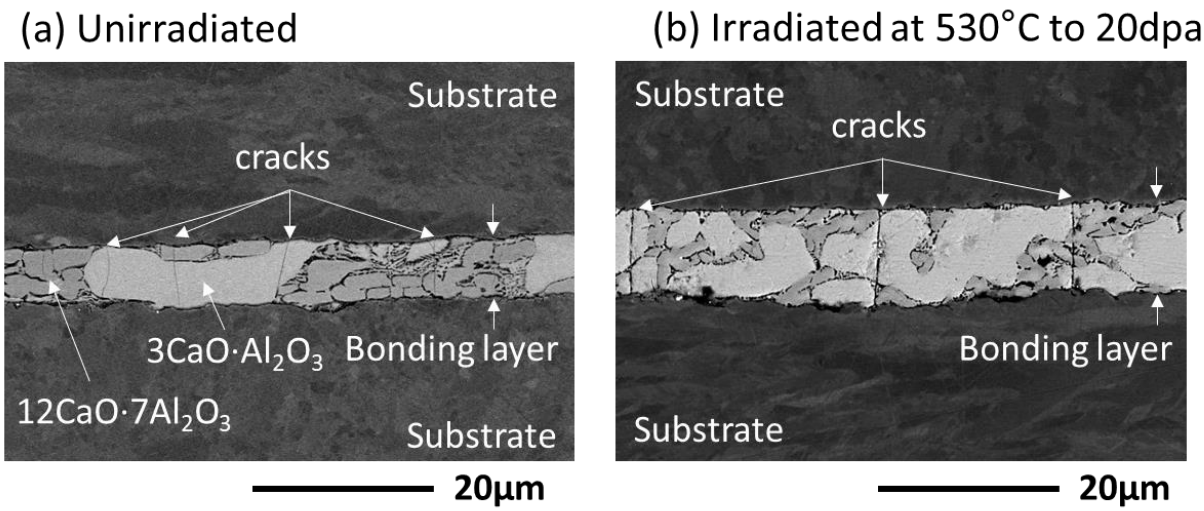

Fig. 12 Backscattered electron images of pressureless CA glass ceramic joint (a) unirradiated and (b) neutron irradiated at 530°C to 20 dpa.

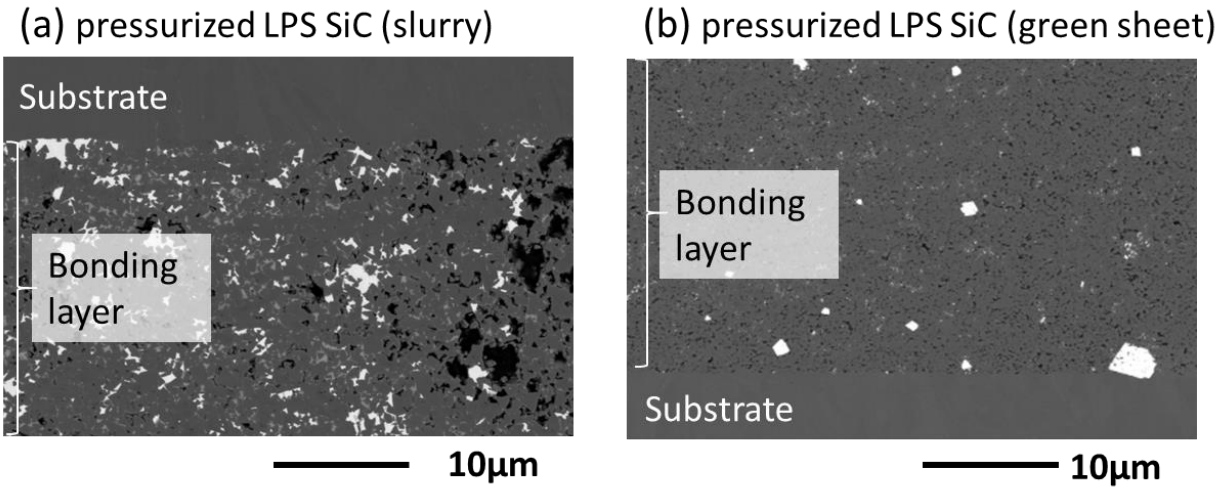

Fig. 13 Backscattered electron images of pressure-assisted LPS SiC joints neutron irradiated at 530°C to 20 dpa: (a) slurry joint and (b) green sheet joint.

Cross-section BSE images of the unirradiated and irradiated hot-pressed MAX-phase joints are shown in Fig. 14. The thickness of the bonding layer was near 15 μm and varied among different locations. The bonding layer was highly dense (>95%), and no macroscopic cracks were found in the unirradiated specimen (Fig. 14a). The irradiated joint showed a microstructure similar to that of the unirradiated joint: a dense bonding layer and no obvious cracking found even after neutron irradiation to 20 dpa (Fig. 14b). Irradiation did not cause any interfacial debonding at the bonding layer or the SiC substrate. SEM observation did not reveal any effects of neutron irradiation on the joint microstructure. The microstructure of the bonding layer was further evaluated by TEM. Fig. 15a and b show bright-field STEM micrographs of the unirradiated and irradiated bonding layers, respectively. Ti_3SiC_2 and SiC phases were randomly

distributed, as seen in the EBSD phase map (Fig. 8b). Most of the interface between the two phases appeared to be intact. In contrast, the interfaces in the irradiated bonding layer showed cavities at the interface of Ti_3SiC_2 and SiC. The cavities were not uniform within the specimen. Fig. 15b represents the most significant case discovered of cavities within an examined area. Irradiation-induced cracking was not observed in the specimen.

Structural ordering/disordering of the Ti_3SiC_2 phase was analyzed by high-resolution (HR) TEM imaging, shown in Fig. 15c and d, since the high-dose radiation effects on this phase were not clear. Both images were taken near the [11-20] zone axis, as shown in the inserted selected area diffraction pattern. The unirradiated Ti_3SiC_2 phase exhibited a relatively ordered lattice, and features of the stacking of basal planes were clearly seen. The layered structure of the irradiated Ti_3SiC_2 was maintained but was disordered compared with that of unirradiated material. The selective area diffraction pattern became diffuse after irradiation, which corresponds to the disordered structure found in the HR-TEM image. This diffuse diffraction pattern indicates significant disordering of basal planes as reported in [25]. Even with the disordered structure, preservation of the laminate structure after irradiation is important for operation of nonlinear fracture behavior of the Ti_3SiC_2 phase [26]. Studying the deformation behavior is beyond the scope of this study. Irradiation-induced cavities were not found within the Ti_3SiC_2 grains. In summary, the major damage in the irradiated MAX-phase joint was local debonding at the interfaces of SiC and Ti_3SiC_2 in the bonding layer. It is worth mentioning that unirradiated Ti_3SiC_2 phase exhibited local lattice disordering even after removal of FIB damage by low energy ion milling (a TEM image of Ti_3SiC_2 with less disordering can be found in [27,28].). Therefore, the radiation damage processes may be different from those operating with higher crystallinity materials studied previously.

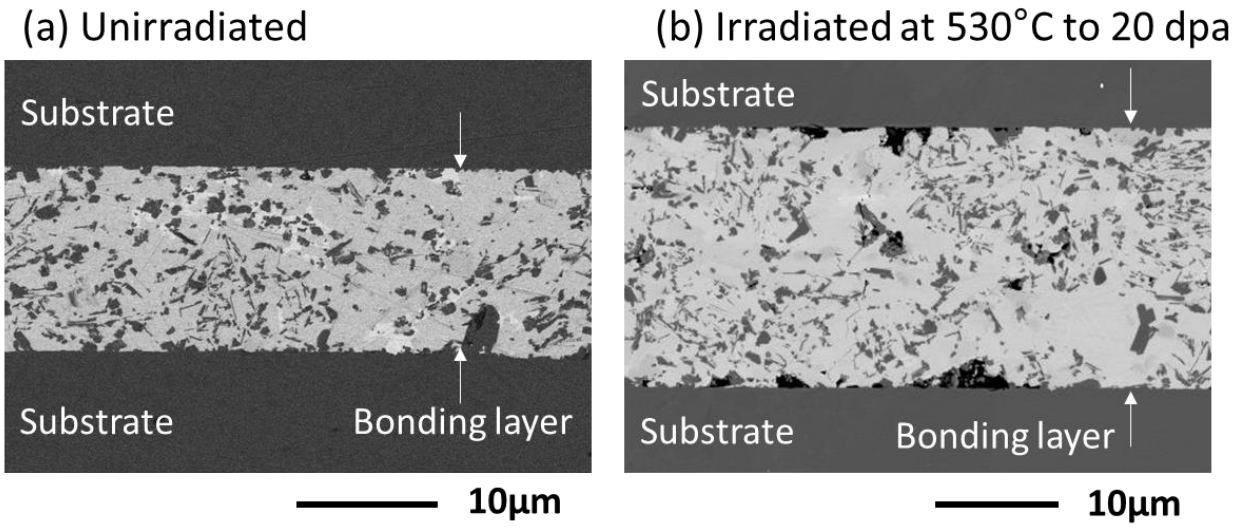

Fig. 14 Backscattered electron images of hot-pressed MAX-phase joints (a) unirradiated and (b) neutron irradiated at 530°C to 20 dpa.

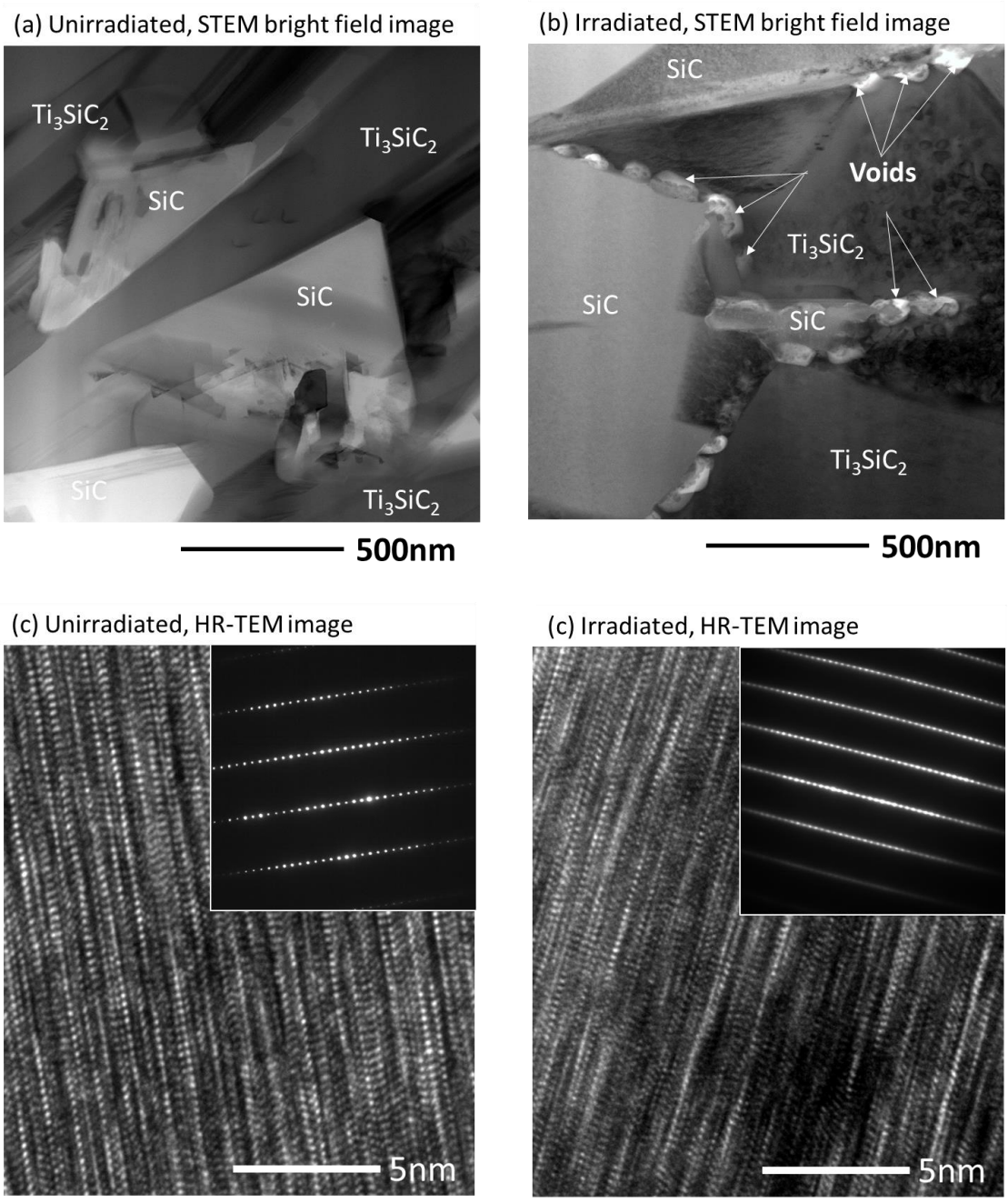

Fig. 15 STEM bright-field images of bonding layer of hot-pressed MAX-phase joints (a) unirradiated and (b) irradiated at 530°C to 20 dpa. HR-TEM images of (c) unirradiated and (d) irradiated Ti_3SiC_2 phase in the joint.

4. Discussion

4.1 Responses of SiC joints to neutron irradiation

The factors influencing radiation effects in the bond zones of SiC joints include changes in the strengths of the substrate and bonding layers due to irradiation damage. In addition, stress attributed to a mismatch in dimensional stability (swelling) between substrate and bonding layer has been reported to affect joint strength [8,9]. Irradiation-induced swelling due to the atomic displacement damage is common for ceramics [29]. Since SiC itself is known to retain its strength even after neutron damage to 28 dpa at 300 and 650°C [30], the strength of the irradiated bonding layer and swelling-induced stresses are the factors to be considered to understand the irradiation effects.

Regarding the LPS-SiC–based joints, it was expected that swelling-induced stress would be minimal because of a limited amount of oxide phases, which is typically <10 vol %. The sensitivity of the strength of sintered SiC ceramics to neutron irradiation varies and depends on the microstructure. Since SiC grains are expected to retain the strength after irradiation, the factor is responses of the oxide phases in the LPS SiC to irradiation. Previous studied indicated importance of the optimization of the secondary phase to be used under irradiation environments; the strength degraded even after it received some neutron damages because of the instability of secondary phases in sintered SiC [31–33]. The strength retention of the pressure-assisted LPS-SiC joints following 20 dpa irradiation indicates that strength of the bonding layer was also preserved. Contrary to expectations based on the high-dose radiation results, the part of the pressure-assisted LPS-SiC joints irradiated at 730°C to 2.3 dpa failed without mechanical testing (Fig. 6). This inconsistency is likely due to deviations in the quality of the joints, rather than an effect of irradiation, because there is no explanation of the significant effect of a 200°C difference in the irradiation temperature on the joint strength. The nonuniform microstructure of these LPS-SiC joints has been reported in our previous study [9]. Such different microstructures did not cause significant deviation of strength before irradiation. Therefore, the failure of the joints is expected to occur during irradiation or disassembly of radiation capsule. It was found that the joints irradiated at 20 dpa were mostly taken from near the center of the as-fabricated plate, whereas the low-dose specimens were taken from near the edge of the joined plate and the unirradiated specimens were randomly taken. It is possible that the nonuniformity of microstructures of the joints was a consequence of the difference in radiation resistance. The overall results for the LPS-SiC–based joints suggest that the torsion shear strength of this type of joint is sensitive to microstructure; the strengths of the as-fabricated material varied depending on the processing (e.g., 319 MPa for the pressure-assisted LPS-SiC [slurry] vs. 114 MPa for the low-pressure LPS-SiC with CP). In addition, the low-pressure LPS-SiC with CP retained its strength following irradiation at 730°C to 2.3dpa, although the other two types of joints showed degradation that was likely due to nonuniform quality of the processing.

The MAX-phase forming joints basically showed a positive response to neutron irradiation; the Ti diffusion bond, pressureless MAX-phase joint, and SPS MAX-phase joint showed no significant strength reduction due to irradiation. The common phenomenon among the joints was cracking or partial debonding within the bond layers during neutron irradiation. One of the sources of the debonding was likely differential swelling between the SiC substrate and the bonding layer (mainly Ti_3SiC_2), as discussed in previous irradiation studies [8,9]. A typical indication of this phenomenon is cracks propagating perpendicular to the joint interface, which

can be explained by larger swelling of the SiC substrate than of the bonding layer. Such swelling-induced stress results in tensile stress in the bonding layer parallel to the joint interface and consequently causes vertical cracks. The swelling mismatch among the phases within the bonding layer is also the reason for the stress buildup and cracking. This is indicated in Fig. 15b, which shows cavity formation (debonding) at the SiC and Ti_3SiC_2 interface. It is also possible that cracking occurred along the grain boundaries of Ti_3SiC_2, since each grain exhibited anisotropic swelling attributed to anisotropic lattice distortion along the *a* and *c* axes [34–36]. Therefore, regardless of the processing route and initial microstructure, irradiation-induced cracking and partial debonding within the bonding layer are challenges for the development of MAX-phase–based joints.

The pressureless CA glass ceramic joint showed no notable microstructural change in SEM images taken following irradiation at 530°C to 20 dpa, although previous work on the same joint type irradiated at 500°C to 3 dpa reported irradiation-induced cracking within the bonding layer because of the differential swelling between the substrate and the glass phases [8]. It is possible that the density of the irradiation-induced cracks was insignificant, so obvious microstructural changes could not be detected because the preexisting cracks and irradiation-induced cracks were mixed at the time of SEM observation. The strength retention after 20 dpa irradiation suggests that the CA glass ceramic itself did not exhibit fatal radiation-induced damage.

4.2 Implication of the results for future research direction

The CA glass ceramics joint, pressure-assisted LPS-SiC joints, and hot-pressed MAX-phase joints did not undergo degradation following high-dose neutron irradiation at 530°C to 20 dpa. The duration of irradiation was ~350 days. This is apparently the first demonstration that SiC joints can withstand such a high neutron damage and long-time exposure to neutrons. This positive result continues to encourage further development of SiC materials for fusion and advanced fission reactor applications, where the core components will experience high neutron dose. Further experiments should be done under neutron irradiation with an application-relevant neutron spectrum when possible, especially for fusion reactor applications, because of the significant impact of the energy spectrum on transmutation events and displacement damage rates [37]. Evaluation of irradiation creep of SiC joints is also critical for applications where the joint is subject to mechanical and/or thermal stresses in service environments. Such stresses can be a limiting factor for MAX-phase–based joints showing irradiation-induced cracking.

It is expected that fabrication and testing SiC components with joined sections will be a focus of research in the near future, since we now know that SiC joints can withstand high-dose neutron irradiation. For example, joining of SiC tubes to end-plugs has recently been demonstrated for fuel cladding applications [38–41], where joining with minimal applied stress is required to avoid damage to the SiC tube. Joining of thin plates, which may be required for fusion reactor applications, is another topic to be studied [4]. The processing requirements unique to the components will bring opportunities for improvement of joining processes. In addition, substrate geometry has been shown to affect the joint strength because of different substrate geometries and different stress states during joining [38]. Another study showed optimization of substrate geometry enabled successful joining of a SiC composite tube to a Zircaloy end-cap [39], illustrating that engineering design, in addition to processing optimization, is required for component fabrication. This kind of engineering effort has been

limited to SiC nuclear applications. Hence, demonstration of robust joints in components will be essential in the next step of joining development.

Another focus area in the development of SiC joints will include chemical compatibility with reactor environments. A fusion reactor blanket may require compatibility of SiC joints with liquid Pb-Li [42]. Fuel cladding of light water reactors requires hydrothermal corrosion resistance of materials during normal operation. Such requirements will limit the selection of SiC bonding layers [43]. Furthermore, the presence of irradiation defects have the potential to accelerate corrosion behavior, depending on the corrosion environment [44,45], so may limit options for joining methods and interlayers. The hermeticity of joints may require SiC joints free of large pores and crack networks. The irradiation-induced cracking found in the MAX-phase–based joints will be a critical issue when a high level of hermeticity is required for SiC components. These considerations will require fabrication and testing of components, an advance beyond only testing plate joints.

5. Conclusions

This study evaluated the response of various SiC joints to neutron irradiation. The findings are summarized as follows.

- The pressure-assisted LPS-SiC–based joints, hot-pressed MAX-phase joints, and pressureless CA glass ceramic joint retained their strength after exposure to neutron irradiation for ~350 days (20 dpa) at 530°C. This demonstration encourages further development of SiC for nuclear applications.

- The strength of the as-fabricated LPS-SiC–based joints was highly dependent on processing and microstructure. In addition, the results indicated that nonuniform microstructures resulted in the joint failures observed after irradiation for both types of pressure-assisted LPS-SiC joints. The joint produced by low-pressure LPS of cold-pressed SiC green body retained its strength following irradiation at 480°C to 2.9 dpa and at 730°C to 2.3 dpa.

- MAX-phase–based joints—including Ti diffusion bond, pressureless MAX-phase bond, and SPS MAX-phase bond—retained their strength following neutron irradiation at ~500°C to 2.9 dpa and at ~700°C to 2.3 dpa, regardless of the differences in the joint microstructures. Irradiation-induced cracking was a common damage process, likely caused by differential swelling between the SiC substrate and the joint phases.

- Processing and evaluation of SiC components fabricated with bonding layers are suggested for future development, expanding beyond the SiC plate joint methods found resistant to neutron irradiation.

Acknowledgments

The work was supported by the US Department of Energy, Office of Fusion Energy Sciences, under contract DE-C05-00OR22725 with UT-Battelle LLC. A portion of this research used resources at the High Flux Isotope Reactor, a DOE Office of Science User Facility operated by the Oak Ridge National Laboratory. The authors wish to thank Frederick Wiffen and Peter Mouche at ORNL for valuable comments for this manuscript.

References

[1] C. Sauder, Ceramic Matrix Composites: Nuclear Applications, in: Ceram. Matrix Compos. Mater. Model. Technol., 2014: pp. 609–646. doi:10.1002/9781118832998.ch22.

[2] C.P. Deck, G.M. Jacobsen, J. Sheeder, O. Gutierrez, J. Zhang, J. Stone, H.E. Khalifa, C.A. Back, Characterization of SiC-SiC composites for accident tolerant fuel cladding, J. Nucl. Mater. 466 (2015) 1–15. doi:10.1016/j.jnucmat.2015.08.020.

[3] L. Giancarli, J.. Bonal, a Caso, G. Le Marois, N.. Morley, J.. Salavy, Design requirements for SiC/SiC composites structural material in fusion power reactor blankets, Fusion Eng. Des. 41 (1998) 165–171. doi:10.1016/S0920-3796(97)00200-7.

[4] A.S.P. Ramírez, A. Caso, L. Giancarli, N. Le Bars, G. Chaumat, J.F. Salavy, J. Szczepanski, Tauro: a ceramic composite structural material self-cooled Pb—17Li breeder blanket concept, J. Nucl. Mater. 233–237 (1996) 1257–1261. doi:10.1016/S0022-3115(96)00147-X.

[5] K.A. Terrani, Accident tolerant fuel cladding development: Promise, status, and challenges, J. Nucl. Mater. 501 (2018) 13–30. doi:10.1016/j.jnucmat.2017.12.043.

[6] L.W. Hobbs, F.W. Clinard, S.J. Zinkle, R.C. Ewing, Radiation effects in ceramics, J. Nucl. Mater. 216 (1994) 291–321. doi:10.1016/0022-3115(94)90017-5.

[7] S.. Fabritsiev, A.. Pokrovsky, D.. Edwards, S.. Zinkle, A.. Rowcliffe, Effect of high-dose neutron irradiation on the mechanical properties and structure of copper alloys and Cu/SS joints for ITER applications, J. Nucl. Mater. 283–287 (2000) 523–527. doi:10.1016/S0022-3115(00)00372-X.

[8] Y. Katoh, L.L. Snead, T. Cheng, C. Shih, W.D. Lewis, T. Koyanagi, T. Hinoki, C.H. Henager, M. Ferraris, Radiation-tolerant joining technologies for silicon carbide ceramics and composites, J. Nucl. Mater. 448 (2014) 497–511. doi:10.1016/j.jnucmat.2013.10.002.

[9] T. Koyanagi, Y. Katoh, J.O. Kiggans, T. Hinoki, H.E. Khalifa, C.P. Deck, C.A. Back, Irradiation resistance of silicon carbide joint at light water reactor–relevant temperature, J. Nucl. Mater. 488 (2017) 150–159. doi:10.1016/j.jnucmat.2017.03.017.

[10] S.J. Zinkle, G.S. Was, Materials challenges in nuclear energy, Acta Mater. 61 (2013) 735–758. doi:10.1016/j.actamat.2012.11.004.

[11] H. Dong, Y. Yu, X. Jin, X. Tian, W. He, W. Ma, Microstructure and mechanical properties of SiC-SiC joints joined by spark plasma sintering, Ceram. Int. 42 (2016) 14463–14468. doi:10.1016/j.ceramint.2016.06.049.

[12] H. Yang, X. Zhou, W. Shi, J. Wang, P. Li, F. Chen, Q. Deng, J. Lee, Y.H. Han, F. Huang, L. He, S. Du, Q. Huang, Thickness-dependent phase evolution and bonding strength of SiC ceramics joints with active Ti interlayer, J. Eur. Ceram. Soc. 37 (2017) 1233–1241. doi:10.1016/j.jeurceramsoc.2016.12.009.

[13] P. Tatarko, Z. Chlup, A. Mahajan, V. Casalegno, T.G. Saunders, I. Dlouhý, M.J. Reece, High temperature properties of the monolithic CVD β-SiC materials joined with a pre-

sintered MAX phase Ti 3 SiC 2 interlayer via solid-state diffusion bonding, J. Eur. Ceram. Soc. 37 (2017) 1205–1216. doi:10.1016/j.jeurceramsoc.2016.11.006.
[14] P. Fitriani, A. Septiadi, J.D. Hyuk, D.-H. Yoon, Joining of SiC monoliths using a thin MAX phase tape and the elimination of joining layer by solid-state diffusion, J. Eur. Ceram. Soc. 38 (2018) 3433–3440. doi:10.1016/j.jeurceramsoc.2018.04.006.
[15] M. Ferraris, M. Salvo, V. Casalegno, S. Han, Y. Katoh, H.C. Jung, T. Hinoki, A. Kohyama, Joining of SiC-based materials for nuclear energy applications, J. Nucl. Mater. 417 (2011) 379–382. doi:10.1016/j.jnucmat.2010.12.160.
[16] C.H. Henager, B.N. Nguyen, R.J. Kurtz, T.J. Roosendaal, B.A. Borlaug, M. Ferraris, A. Ventrella, Y. Katoh, Modeling and testing miniature torsion specimens for SiC joining development studies for fusion, J. Nucl. Mater. 466 (2015) 253–268. doi:10.1016/j.jnucmat.2015.07.044.
[17] C.H. Henager, R.J. Kurtz, Low-activation joining of SiC/SiC composites for fusion applications, J. Nucl. Mater. 417 (2011) 375–378. doi:10.1016/j.jnucmat.2010.12.084.
[18] S. Grasso, P. Tatarko, S. Rizzo, H. Porwal, C. Hu, Y. Katoh, M. Salvo, M.J. Reece, M. Ferraris, Joining of β-SiC by spark plasma sintering, J. Eur. Ceram. Soc. 34 (2014) 1681–1686. doi:10.1016/j.jeurceramsoc.2013.12.023.
[19] W.H. Martin, A.M. Price, Determination of dose and temperature in graphite irradiation experiments in the dounreay fast reactor, J. Nucl. Energy. 21 (1967) 359–371. doi:10.1016/0022-3107(67)90116-5.
[20] E. Gomez, J. Echeberria, I. Iturriza, F. Castro, Liquid phase sintering of SiC with additions of Y2O3, Al2O3 and SiO2, J. Eur. Ceram. Soc. 24 (2004) 2895–2903. doi:10.1016/j.jeurceramsoc.2003.09.002.
[21] A. Noviyanto, D.-H. Yoon, Metal oxide additives for the sintering of silicon carbide: Reactivity and densification, Curr. Appl. Phys. 13 (2013) 287–292. doi:10.1016/j.cap.2012.07.027.
[22] B. V Cockeram, The Diffusion Bonding of Silicon Carbide and Boron Carbide Using Refractory Metals, (n.d.). https://www.osti.gov/servlets/purl/755392 (accessed March 1, 2018).
[23] M. Naka, J. Feng, J.C. Schuster, Phase stability of SiC against Ti at high temperature, Vacuum. 83 (2008) 223–225. doi:10.1016/j.vacuum.2008.04.001.
[24] V. Casalegno, S. Kondo, T. Hinoki, M. Salvo, A. Czyrska-Filemonowicz, T. Moskalewicz, Y. Katoh, M. Ferraris, CaO-Al2O3 glass-ceramic as a joining material for SiC based components: A microstructural study of the effect of Si-ion irradiation, J. Nucl. Mater. 501 (2018) 172–180. doi:10.1016/j.jnucmat.2018.01.033.
[25] D.J. Tallman, L. He, J. Gan, E.N. Caspi, E.N. Hoffman, M.W. Barsoum, Effects of neutron irradiation of Ti3SiC2 and Ti3AlC2 in the 121–1085 °C temperature range, J. Nucl. Mater. 484 (2017) 120–134. doi:10.1016/j.jnucmat.2016.11.016.
[26] M.W. Barsoum, M. Radovic, Elastic and Mechanical Properties of the MAX Phases, Annu. Rev. Mater. Res. 41 (2011) 195–227. doi:10.1146/annurev-matsci-062910-100448.
[27] K. Buchholt, R. Ghandi, M. Domeij, C.-M. Zetterling, J. Lu, P. Eklund, L. Hultman, A.L. Spetz, Ohmic contact properties of magnetron sputtered Ti3SiC2 on n- and p-type 4H-silicon carbide, Appl. Phys. Lett. 98 (2011) 042108. doi:10.1063/1.3549198.
[28] Q. Huang, R. Liu, G. Lei, H. Huang, J. Li, S. He, D. Li, L. Yan, J. Zhou, Q. Huang, Irradiation resistance of MAX phases Ti 3 SiC 2 and Ti 3 AlC 2 : Characterization and comparison, J. Nucl. Mater. 465 (2015) 640–647. doi:10.1016/j.jnucmat.2015.06.056.

[29] R.J.. Konings, K. Bakker, J.. Boshoven, R. Conrad, H. Hein, The influence of neutron irradiation on the microstructure of Al2O3, MgAl2O4, Y3Al5O12 and CeO2, J. Nucl. Mater. 254 (1998) 135–142. doi:10.1016/S0022-3115(97)00355-3.
[30] Y. Katoh, T. Nozawa, L.L. Snead, K. Ozawa, H. Tanigawa, Stability of SiC and its composites at high neutron fluence, J. Nucl. Mater. 417 (2011) 400–405. doi:10.1016/j.jnucmat.2010.12.088.
[31] R.B. Matthews, Irradiation damage in reaction-bonded silicon carbide, J. Nucl. Mater. 51 (1974) 203–208. doi:10.1016/0022-3115(74)90003-8.
[32] J.C. CORELLI, J. HOOLE, J. LAZZARO, C.W. LEE, Mechanical, Thermal, and Microstructural Properties of Neutron-Irradiated SiC, J. Am. Ceram. Soc. 66 (1983) 529–538. doi:10.1111/j.1151-2916.1983.tb10596.x.
[33] T. Iseki, T. Maruyama, T. Yano, T. Suzuki, T. Mori, Effects of neutron irradiation and subsequent annealing on strength and toughness of SiC ceramics, J. Nucl. Mater. 170 (1990) 95–100. doi:10.1016/0022-3115(90)90330-P.
[34] D.J. Tallman, E.N. Hoffman, E.N. Caspi, B.L. Garcia-Diaz, G. Kohse, R.L. Sindelar, M.W. Barsoum, Effect of neutron irradiation on select MAX phases, Acta Mater. 85 (2015) 132–143. doi:10.1016/j.actamat.2014.10.068.
[35] D.W. Clark, S.J. Zinkle, M.K. Patel, C.M. Parish, High temperature ion irradiation effects in MAX phase ceramics, Acta Mater. 105 (2016) 130–146. doi:10.1016/j.actamat.2015.11.055.
[36] Q. Qi, G.J. Cheng, L.Q. Shi, D.J. O'Connor, B.V. King, E.H. Kisi, Damage accumulation and recovery in C+-irradiated Ti3SiC2, Acta Mater. 66 (2014) 317–325. doi:10.1016/j.actamat.2013.11.019.
[37] H.L. Heinisch, L.R. Greenwood, W.J. Weber, R.E. Williford, Displacement damage in silicon carbide irradiated in fission reactors, J. Nucl. Mater. 327 (2004) 175–181. doi:10.1016/j.jnucmat.2004.02.012.
[38] H.E. Khalifa, C.P. Deck, O. Gutierrez, G.M. Jacobsen, C.A. Back, Fabrication and characterization of joined silicon carbide cylindrical components for nuclear applications, J. Nucl. Mater. 457 (2015) 227–240. doi:10.1016/j.jnucmat.2014.11.071.
[39] H. Serizawa, N. Nakazato, Y. Sato, M. Tsukamoto, J. Park, H. Kishimoto, Experimental studies on joinability of zircaloy and SiC/SiC composite with titanium powder, Int. J. Ceram. Eng. Sci. 1 (2019) 57–63. doi:10.1002/ces2.10010.
[40] E.D. Herderick, Novel silicon carbide joining for new generation of accident-tolerant nuclear fuels, Am. Ceram. Soc. Bull. 92 (2013) 32–35.
[41] M. Herrmann, W. Lippmann, A. Hurtado, High-temperature stability of laser-joined silicon carbide components, J. Nucl. Mater. 443 (2013) 458–466. doi:10.1016/j.jnucmat.2013.07.067.
[42] C. Park, T. Nozawa, R. Kasada, S. Tosti, S. Konishi, H. Tanigawa, The effect of wall flow velocity on compatibility of high-purity SiC materials with liquid Pb-Li alloy by rotating disc testing for 3000 h up to 900 °C, Fusion Eng. Des. 136 (2018) 623–627. doi:10.1016/j.fusengdes.2018.03.042.
[43] J.D. Stempien, D.M. Carpenter, G. Kohse, M.S. Kazimi, Characteristics of Composite Silicon Carbide Fuel Cladding after Irradiation under Simulated PWR Conditions, Nucl. Technol. 183 (2013) 13–29. doi:10.13182/NT12-86.
[44] P. Deng, Q. Peng, E.-H. Han, W. Ke, C. Sun, Z. Jiao, Effect of irradiation on corrosion of 304 nuclear grade stainless steel in simulated PWR primary water, Corros. Sci. 127 (2017)

91–100. doi:10.1016/j.corsci.2017.08.010.
[45] J. Li, H. Huang, Q. Huang, M. Tang, B. Zhao, G. Ji, W. Zhang, R. Xie, L. Yan, Effect of irradiation damage on corrosion of 4H-SiC in FLiNaK molten salt, Corros. Sci. 125 (2017) 194–197. doi:10.1016/j.corsci.2017.05.028.